# Expanded View Figures

**Figure EV1. MASTL modulates AKT activity in response to glucose and insulin independently of its mitotic function.**

A Cell cycle analysis in RNA interference MASTL-depleted cells. MDA-MB-231 cells were infected with shRNAs specific for *MASTL* (+) or scramble (−) as a control, and the cell cycle was analyzed 48, 72, and 96 h later. Mitotic cells were scored using immunodetection of P-S10-H3 (pH3) and total DNA was stained with Hoechst 33342 followed by flow cytometry analysis. The plot shows the quantification of the different phases of the cell cycle in control and *MASTL*-depleted cells. Data are mean + SEM of three independent experiments. Significance was determined by two-way ANOVA comparing MASTL-depleted cells versus control cells (not significant at any time point). Representative immunoblotting to monitor MASTL depletion is also shown. α-Tubulin was used as a loading control.

B Immunoblot analysis of asynchronous (Asyn.) MDA-MB-231 cells subjected to different starvations [elimination of fetal bovine serum (FBS), glucose (Gluc.), amino acids (AA), or oxygen] using the indicated antibodies in the absence (−) or presence (+) of shRNAs against *MASTL*. *Indicates unspecific band. β-Actin was used as a loading control.

C Cell cycle analysis in inducible CRISPR-Cas9 MASTL-deleted cells. *MASTL* was ablated in MDA-MB-231 cells using the *isgMASTL* system, and cell cycle was analyzed 48, 72, and 96 h after doxycycline treatment. Mitotic cells were scored using immunodetection of P-S10-H3 (pH3) and total DNA was stained with Hoechst 33342 followed by flow cytometry analysis. The graph shows the quantification of the different phases of the cell cycle in control and *MASTL*-depleted cells. Data are mean + SEM of three independent experiments. Significance was determined by two-way ANOVA comparing MASTL-depleted cells versus control cells (*$P < 0.05$ at 96 h for subG1 and > 4N). Representative immunoblotting to monitor MASTL depletion is also shown. α-Tubulin was used as a loading control.

D Control of the Dox and Cas9 expression in the MDA-MB-231 *isgMASTL* system using a control clone that expresses Cas9 alone (iCas9). The same protocol as in Fig 1B was followed.

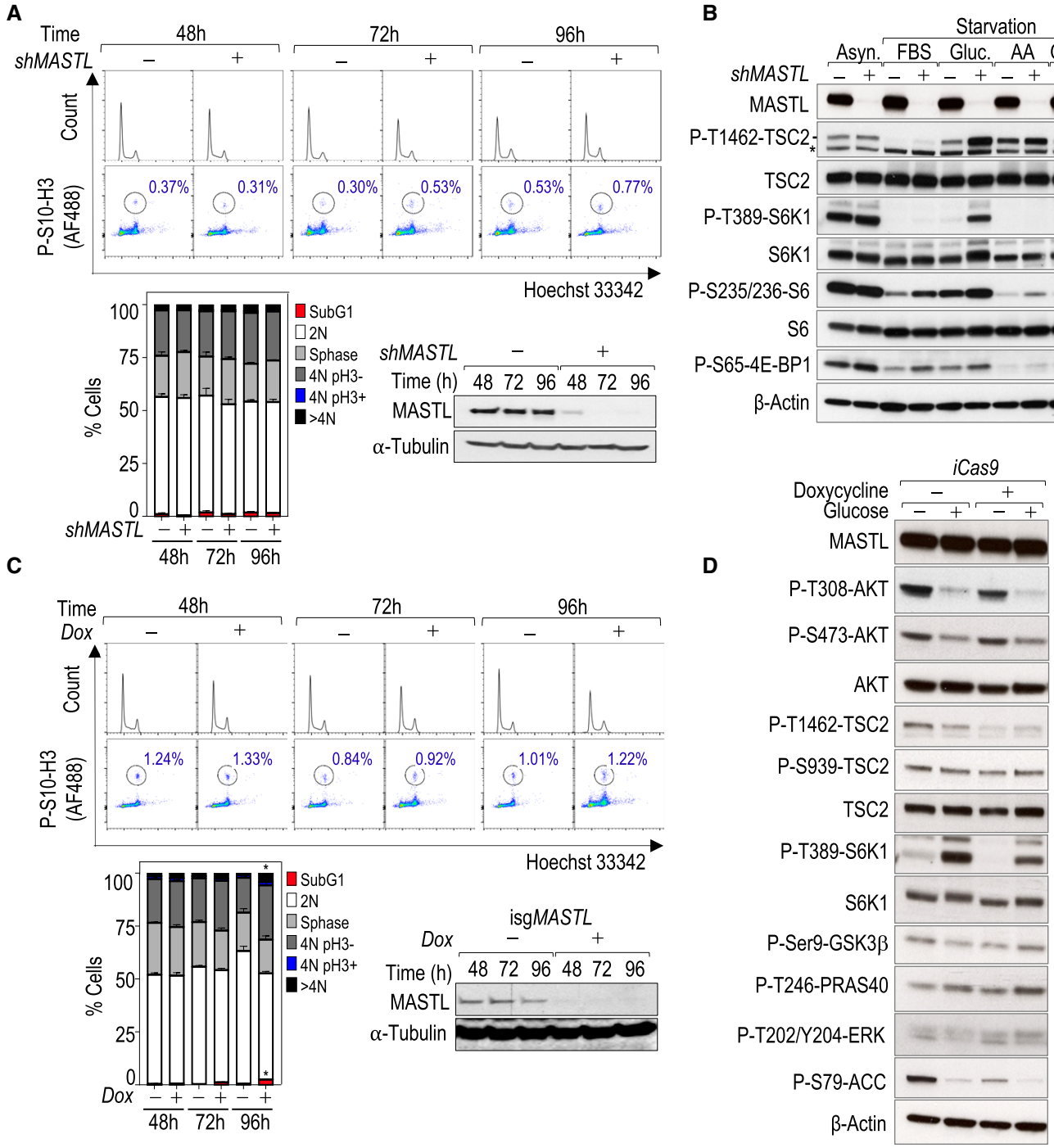


**Figure EV1.**

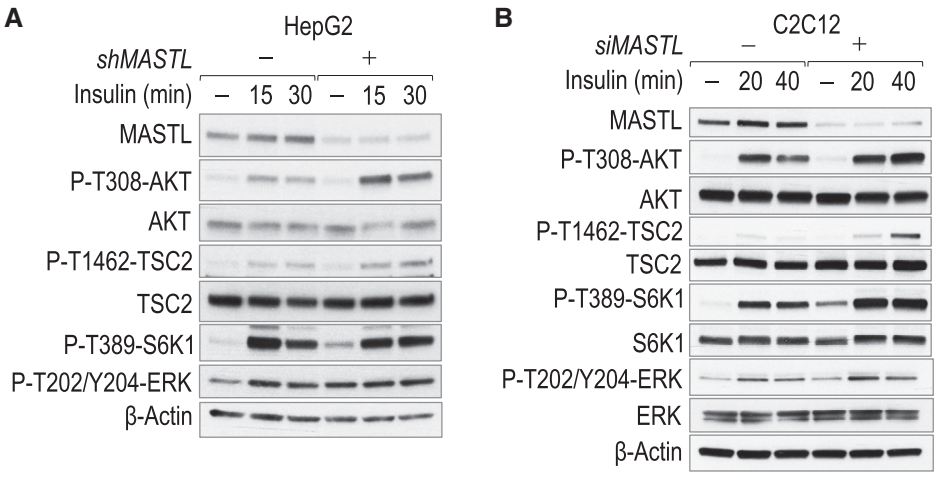


**Figure EV2. MASTL modulates AKT activity in response to insulin.**

A HepG2 cells were depleted of MASTL, and serum was starved and stimulated with insulin for the indicated periods of time, following the protocol shown in Fig 1A. Whole-cell lysates were probed with the indicated antibodies.

B Mouse C2C12 myoblasts were depleted of Mastl using specific siRNAs. Forty-eight hours after transfection, cells were placed in differentiation medium for 24 h (2% horse serum), serum-starved for 5 h, and stimulated with insulin for the indicated periods of time. Whole-cell lysates were probed with the indicated antibodies.

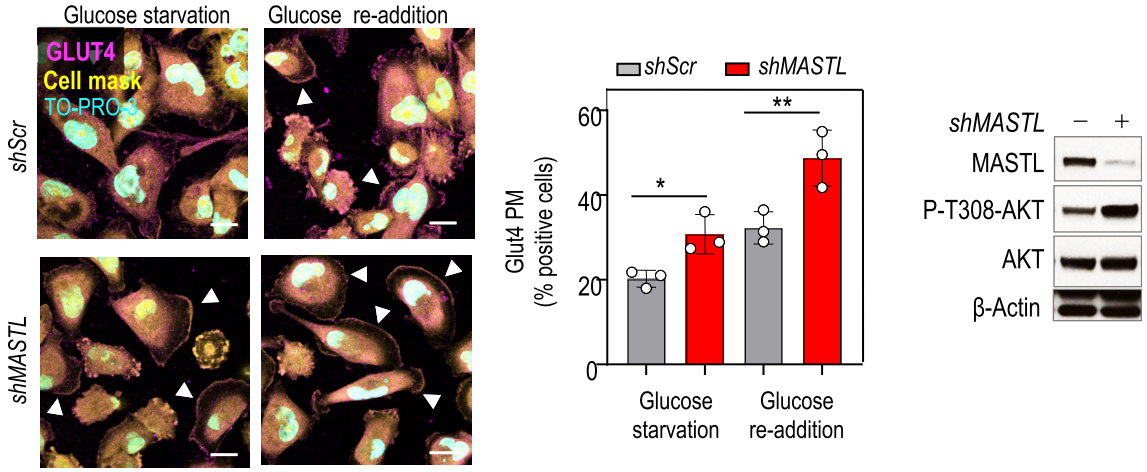


**Figure EV3. Effect of MASTL depletion on cellular metabolism.**

MASTL was knocked down using shRNAs for *MASTL* (+) and scramble shRNA (−) as a control in MDA-MB-231 cells, and immunofluorescence for GLUT4 (magenta) in conditions of glucose starvation and re-addition was performed. TO-PRO-3 (DNA) is in cyan and a cell mask is in yellow. Arrowheads indicate positive cells for GLUT4 enrichment at the plasma membrane (PM). Scale bars, 10 μm. The graph shows the quantification of the percentage of cells positive for GLUT4 at the PM. The bar chart displays mean data ± SEM from thee independent experiments. Significance was determined by one-way ANOVA (*$P < 0.05$; **$P < 0.01$). Control immunoblotting is shown in conditions of glucose re-addition for the indicated antibodies.

**Figure EV4. Effect of MASTL ablation on glucose metabolism *in vivo*.**

A Survival curve of adult *Mastl*(+/Δ) ($n = 11$) and *Mastl*(Δ/Δ) ($n = 14$) mice after continuous tamoxifen treatment. No significant differences were found in the log-rank (Mantel–Cox) test.

B Plots representing the relative body weight of the mice included in the GTT assay from Fig 4. Body weight gain after 9 weeks of HFD (Left); body weight loss 1 week after tamoxifen injection (Middle); body weight loss after 16 h fasting (Right). $n = 6$ *Mastl*(+/+) and $n = 11$ *Mastl*(Δ/Δ). Error bars indicate SEM (unpaired student's *t*-test).

C Representative images of the intestine from *Mastl*(+/+) and *Mastl*(Δ/Δ) mice showing the normal architecture of the epithelia by hematoxylin and eosin (H&E) staining (upper panel) and similar levels of proliferation (Ki67 staining, lower panels). Scale bars, 25 μm.

D Insulin tolerance test (ITT) in *Mastl*(+/+) ($n = 6$) and *Mastl*(Δ/Δ) ($n = 11$) mice. Data are mean ± SEM; ns, not significant; two-way ANOVA.

E Immunoblot with the indicated antibodies in muscle tissues from *Mastl*(+/+) ($n = 8$) and *Mastl*(Δ/Δ) ($n = 7$) mice. Mice were fasted overnight for 16 h and sacrificed for sample collection. Quantification of the relative fold change signal of phospho-AKT T308 and phospho-AKT S473. Data are mean ± SEM; $^{**}P < 0.01$; $^{***}P < 0.001$, unpaired Student's *t*-test.

F RT–qPCR analysis of *Mastl* mRNA in liver tissues from *Mastl*(+/+) and *Mastl*(Δ/Δ) mice fasted overnight for 16 ($n = 7$ mice/genotype), and injected intraperitoneally with glucose (2 g/kg body) ($n = 3$ mice/genotype), or re-fed for 2 h and sacrificed 30 min later for sample collection refeeding conditions ($n = 4$ mice/genotype). *Hprt1* was used as a housekeeping gene to normalize *Mastl* expression level. Plots show the mean + SEM; ns, not significant; $^{*}P < 0.05$; $^{**}P < 0.01$, unpaired Student's *t*-test.

G RT–qPCR analysis of *Mastl* mRNA in muscle tissues from *Mastl*(+/+) and *Mastl*(Δ/Δ) mice fasted overnight for 16 ($n = 8$ control mice and $n = 5$ *Mastl* KO mice), and injected intraperitoneally with glucose (2 g/kg body) ($n = 4$ control mice and $n = 3$ *Mastl* KO mice), or re-fed for 2 h, and sacrificed 30 min later for sample collection refeeding conditions ($n = 3$ mice/genotype). *Hprt1* was used as a housekeeping gene to normalize *Mastl* expression level. Plots show the mean + SEM; ns, not significant; $^{*}P < 0.05$, unpaired Student's *t*-test.

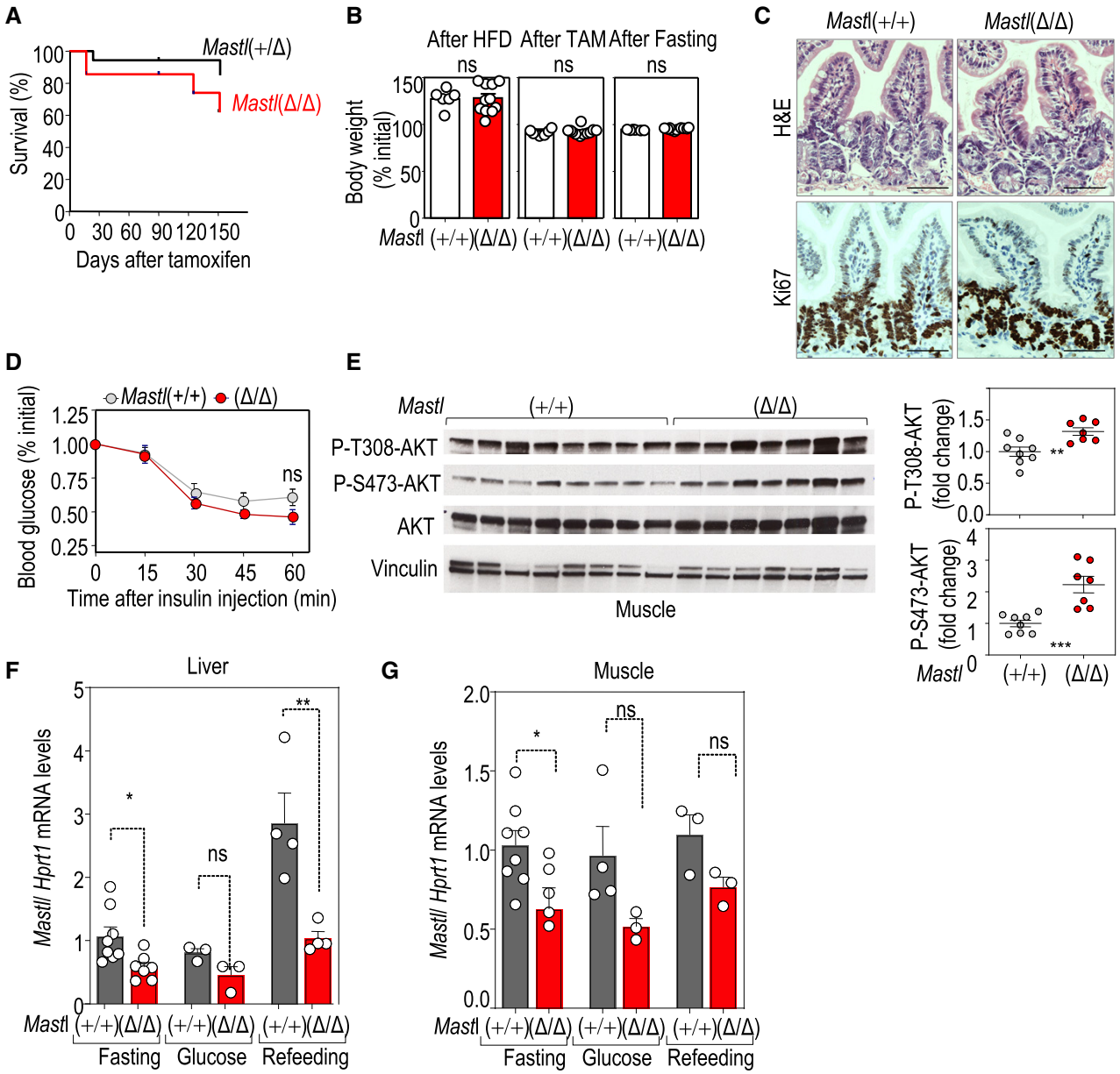
A
Mastl(+/Δ)
Mastl(Δ/Δ)
Survival (%)
Days after tamoxifen
B
After HFD
After TAM
After Fasting
ns
Body weight (% initial)
Mastl (+/+)(Δ/Δ) (+/+)(Δ/Δ) (+/+)(Δ/Δ)
C
Mastl(+/+)
Mastl(Δ/Δ)
H&E
Ki67
D
Mastl(+/+) (Δ/Δ)
Blood glucose (% initial)
Time after insulin injection (min)
E
Mastl (+/+) (Δ/Δ)
P-T308-AKT
P-S473-AKT
AKT
Vinculin
Muscle
P-T308-AKT (fold change)
P-S473-AKT (fold change)
F
Liver
Mastl/ Hprt1 mRNA levels
Fasting Glucose Refeeding
G
Muscle

**Figure EV4.**

**Figure EV5. Regulation of MASTL activity by mTORC1.**

A *In vitro* kinase assay using GFP-hMASTL immunocomplexes from asynchronous TSC2 knockout cells (*sgTSC2*) or control cells treated with the indicated inhibitors for 1 h. Immunoprecipitation of GFP alone was used as a control. GST-ARPP19 was used as a substrate. The upper panel shows the radiograph of ARPP19 phosphorylation in the different conditions accompanied by the immunoblots of the whole-cell extracts. Quantification of the relative kinase activity of MASTL is shown in the lower graph, in which MASTL activity in sg*TSC2* cells was set as 1. Data are mean ± SEM from four independent experiments. Significance determined by paired Student's *t*-test (ns, not significant; **P* < 0.05; ***P* < 0.01).

B A homology structural model showing the position of S875 and S878 in the regulatory C-tail domain of human MASTL. Ribbon diagram of the MASTL kinase domain (without the residues 181–727 coding for the NCMR; left panel) in complex with ATP. The protein fold displays the standard bilobal structure (N-lobe and C-lobe) with its respective AGC C-tail (shown in brown). Please see the associated key for common structural kinase domain components. Molecular details for the phospho-binding pocket of MASTL (right panel). Using the homology-modeled AGC C-tail of MASTL, it is possible to determine that amino acids Lys48, Lys65, Asn104, and Asn105 (stick representation) are positioned such that they could interact with the phosphorylated tail/liker reside (pSer875) and the mTOR-phosphorylation site (pSer878). Note, in both panels, the MASTL protein has been homology-modeled using MODELLER based on the structures of MASTL (PDB 5LOH2; https://www.rcsb.org/) for the kinase domain and of PKA and RSK2 (PDBs 1ATP and 4EL9, respectively) for the AGC C-tail.

C Mouse embryonic fibroblasts (MEFs) were synchronized in G0 by serum starvation and then released for 6 h in the presence of serum (G1). Endogenous Mastl was immunoprecipitated with a specific antibody against Mastl (Abgent) and subjected to mass spectrometry to identify phosphorylated residues in Mastl in the indicated conditions. The upper panel shows the immunoblot of the immunoprecipitates and inputs probed with the indicated antibodies. The lower graphs show the relative quantification of the indicated phosphopeptides in both conditions.

D A model for the role of the MASTL-ENSA/ARPP19-PP2A/B55 pathway in the negative feedback loop that controls AKT activity in response to mTORC1-S6K1 signaling. For simplicity, only the phosphoresidues in the negative feedback loop are shown.

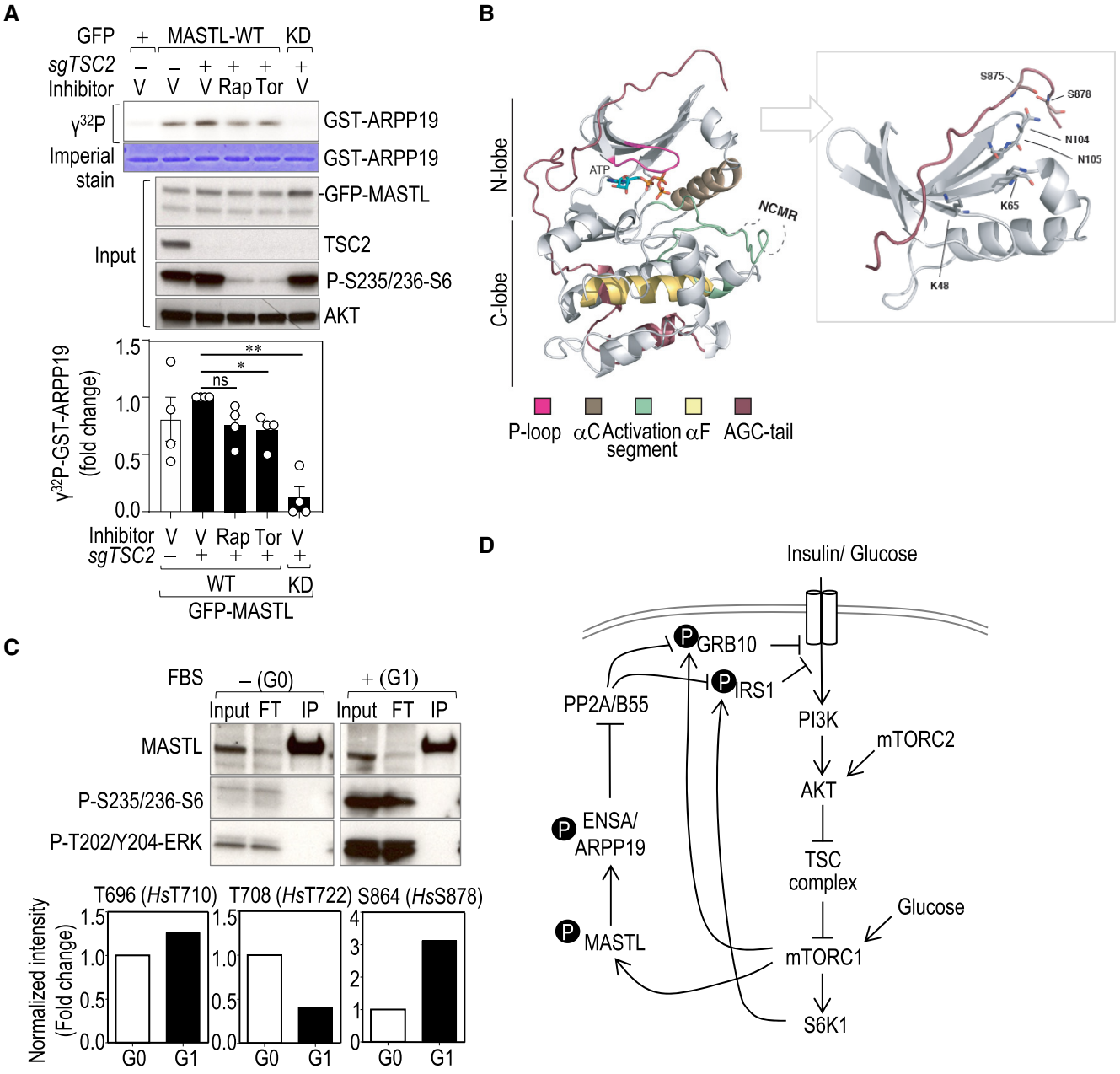
A
GFP + MASTL-WT KD
sgTSC2 – – + + + +
Inhibitor V V V Rap Tor V
γ32P
GST-ARPP19
Imperial stain
GST-ARPP19
GFP-MASTL
Input
TSC2
P-S235/236-S6
AKT
γ32P-GST-ARPP19 (fold change)
1.5
1.0
0.5
0.0
**
*
ns
Inhibitor V V Rap Tor V
sgTSC2 – + + + +
WT KD
GFP-MASTL
B
N-lobe
C-lobe
ATP
NCMR
S875
S878
N104
N105
K65
K48
P-loop αC Activation segment αF AGC-tail
C
FBS – (G0) + (G1)
Input FT IP Input FT IP
MASTL
P-S235/236-S6
P-T202/Y204-ERK
T696 (HsT710) T708 (HsT722) S864 (HsS878)
Normalized intensity (Fold change)
1.5
1.0
0.5
0.0
4
3
2
1
0
G0 G1 G0 G1 G0 G1
D
Insulin/ Glucose
GRB10
IRS1
PP2A/B55
PI3K
mTORC2
AKT
ENSA/ ARPP19
TSC complex
Glucose
MASTL
mTORC1
S6K1

**Figure EV5.**